Nanoscale

PAPER

View Article Online
View Journal | View Issue

Cite this: *Nanoscale*, 2024, **16**, 17559

X-ray photoelectron spectroscopy of high-throughput mechanically exfoliated van der Waals materials†

Nuria Jiménez-Arévalo, *[a] Carlo Mariani, [a,b] Fabrice Leardini, [c] Francesco Pandolfi, [b] Ilaria Rago [b] and Riccardo Frisenda *[a]

Received 11th July 2024,
Accepted 27th August 2024

DOI: 10.1039/d4nr02882a

rsc.li/nanoscale

X-ray photoelectron spectroscopy (XPS) is a widely used and easy accessible characterisation technique for investigating the chemical composition of materials. However, investigating the composition of van der Waals (vdW) flakes by XPS is challenging due to the typical spot size of XPS setups compared to the dimensions of the flakes, which are usually one thousand times smaller than the spot size. In this work, we demonstrate the feasibility of quantitative elemental analysis of vdW materials by using high-throughput mechanical exfoliations, which favour the coverage of arbitrary substrates with flakes of areas of the order of the cm^2 using minimal quantities of materials (about 10 μg). We have analysed the chemical composition of MoS_2, graphite, WSe_2 and $FePS_3$. The high-resolution measurement of their main core levels through XPS demonstrates the absence of significant contamination during the transfer method. In the case of air-sensitive $FePS_3$, the glove box fabrication and its degradation in air are discussed. Overall, this research opens the possibility of evaluating the purity of commercial or lab-synthesized flakes and paves the way towards a more systematic comparison between the composition of vdW materials produced and used among different laboratories.

Introduction

Van der Waals (vdW) materials, such as graphite or transition metal dichalcogenides (TMDCs), have garnered significant interest due to their outstanding optical, electrical[1–5] and mechanical[6–8] properties. Owing to their layered structure, these materials can be mechanically exfoliated, producing excellent-quality two-dimensional (2D) flakes, which are homogenous in thickness and defect-free.[9–12] Nevertheless, the typical size of exfoliated flakes is of the order of 100 μm^2, thus hindering the scalability and applicability of these compounds outside the laboratory. Consequently, many efforts have been directed towards scaling up the mechanical exfoliation methods to produce large quantities of 2D flakes.[13–16] A recent research study by Y. Sozen *et al.*[15] has reported a method to produce massive parallel exfoliation of vdW materials using a roll-to-roll set-up. This technique has facilitated the production of densely packed mechanically exfoliated vdW material flakes with large lateral sizes on arbitrary substrates.

X-ray photoelectron spectroscopy (XPS) is a widely used and powerful characterisation technique for investigating the elemental abundances and chemical composition of materials.[17–19] However, in conventional laboratory settings, the spatial resolution of XPS typically exceeds 10^{-1} mm^2, which is much larger than the typical size of 2D flakes. Thus, synchrotron radiation is often employed for this purpose,[20] even though it is less accessible to a general audience and not suitable for rapid surveys of the chemical composition of the 2D flakes. Therefore, the challenge of easily investigating the elemental composition of mechanically exfoliated 2D flakes using conventional XPS apparatus remained unsolved.

In this work, we employed a similar technique to that developed by Y. Sozen *et al.*[15] to characterise with XPS the composition of various mechanically exfoliated vdW materials transferred on large-area substrates (of the order of 1 cm^2), using minimal quantities of the chosen material (approximately 10 μg). This approach enables the possibility of assessing the purity of commercial vdW materials, investigating composition modifications induced by different techniques, or the characterisation of laboratory-produced materials that are typically produced in small quantities. Also, it can ease the comparison of the same 2D material exfoliated or produced by different research groups.

[a]*Dipartimento di Fisica, Università di Roma "La Sapienza", 00185 Rome, Italy. E-mail: nuria.jimenezarevalo@uniroma1.it, riccardo.frisenda@uniroma1.it*
[b]*Istituto Nazionale di Fisica Nucleare Sezione di Roma, 00185 Rome, Italy*
[c]*Departamento de Física de Materiales, Universidad Autónoma de Madrid, 28049 Madrid, Spain*

† Electronic supplementary information (ESI) available. See DOI: https://doi.org/10.1039/d4nr02882a

Our findings were validated through a thorough characterisation of MoS_2 as the case of study, as well as by the analysis of other vdW materials such as graphite (Gr), WSe_2, and $FePS_3$. Notably, the characterisation of air-sensitive $FePS_3$ highlights the capability of performing this transfer method under an inert atmosphere. Additionally, in our investigation, we show the fast degradation of this compound when stored in air by the observation of oxide species by XPS. This underscored the importance of carefully managing environmental factors to maintain the stability of air-sensitive vdW materials.

Overall, this research introduces a valuable tool for characterising vdW material purity and quality, without the necessity of large quantities of materials and can pave the way to a more systematic comparison of vdW materials produced in different laboratories.

Experimental method

Chemicals and substrates

For the MoS_2 and graphite exfoliations, bulk natural molybdenite (Moly Hill mine) and graphite (Pro Graphite) were used. WSe_2 was supplied by HQGraphene. $FePS_3$ was synthesized at the MIRE Lab from Universidad Autónoma de Madrid by chemical vapor transport method. Here, a stoichiometric mixture of Fe (Goodfellow, 99.0% purity), S (Merck, 99.99% purity) and P_2S_5 (Sigma Aldrich, 99% purity) powders was placed into a quartz ampoule inside an Ar-filled glove box (Jacomex Model Campus). The open side of the ampoule was connected to a valve with Viton fittings and taken out of the glove box. Then it was connected to a high vacuum pump (in the 10^{-6} mbar range) and sealed using a blowtorch. To avoid the sublimation of P_2S_5 precursor during sealing in vacuum, the bottom part of the ampoule was immersed in a liquid nitrogen bath. Afterwards, the sealed ampoule was placed in a two-zones split tube furnace (Carbolite). The two extremes of the ampoule were heated at 740 °C and 680 °C during 100 h, respectively. $FePS_3$ flakes were collected at the cold side of the ampoule.

Sample preparation

A few micrograms of the target vdW materials were placed on Nitto tape. Several manual exfoliations were produced until a homogeneous distribution similar to the one reported in[15] was obtained. The Nitto tape with the flakes was then stuck to the Si wafer (⟨111⟩, p-type, 1 Ω cm, with a native SiO_2 layer on top) and annealed at 110 °C for 5 minutes. After the sample cooled down, the Nitto tape was removed. This process can be repeated to increase the coverage. See Fig. S1† for a detailed schematic of the procedure.

Morphological characterisation

The morphology of the Si sample covered by the flakes has been investigated by optical microscopy using a Motic BA 340 microscope and by scanning electron microscopy (SEM) with a field emission Zeiss Auriga 405 instrument (operated at 3 kV and 4.3 mm of working distance) at the CNIS Laboratory of Sapienza University of Rome. A further morphological characterisation has been performed by atomic force microscopy (AFM) using a Park Systems NX10 AFM in tapping mode operated in air. We used a Nanosensors PPP-NCHR AFM tip and collected micrographs of 512 × 512 pixels at a measurement rate of 0.1 Hz (that corresponds approximately to speeds of 5 μm s^{-1}).

X-ray photoelectron spectroscopy

The composition of the flakes was investigated by XPS. The characterisation was carried out in an ultra-high vacuum (UHV) chamber with a base pressure in the low 10^{-10} mbar range. Photoelectrons were excited with an Al Kα (1468.7 eV) or Mg Kα (1253.6 eV) photon source and measured with a hemispherical electron analyser (VG Microtech Clam-2) in pass energy (PE) mode, with PE = 50 eV. Binding energy was calibrated by acquiring the Au $4f_{7/2}$ (84.0 eV) core level after each measurement using a reference gold film (cleaned by Argon ion sputtering in UHV) mounted next to the investigated sample and in good electrical contact with it. The software used to fit the single components of the core-levels was XPST (X-ray Photoelectron Spectroscopy Tools) implemented in Igor Pro (WaveMetrics, Inc.).

Samples were held to the Mo sample holder using Ta strips and were annealed at 120 °C for at least 12 h in UHV before XPS measurements to remove eventual airborne contaminants.

Results and discussion

Molybdenum disulfide (MoS_2) has been used as the first case of study of the viability of employing the large-area mechanical exfoliation and transfer method for XPS analysis. Three transfers, each one lasting 5 minutes at 110 °C, were conducted on the same Si wafer to obtain a sample of high-density tightly packed flakes. The morphological characterisation of this sample is presented in Fig. 1, with additional information available in Fig. S2† regarding the intermediate transfers.

In Fig. 1a, a photograph of the sample under research is given. The sample is approximately 1 cm^2 large. In the upper and lower parts of the photograph the Si substrate is revealed; meanwhile, the central part of the sample is covered with the MoS_2 flakes. Fig. 1b offers a schematic representation of the deposited MoS_2 flakes from different angles. Microscale characterisation (Fig. 1c–e) reveals uncovered spaces where the substrate remains exposed, schematically illustrated in Fig. 1b. Both optical microscopy (OM) and scanning electron microscopy (SEM) images, performed in the same sample region, show contrast between the MoS_2 and the substrates. Nevertheless, it is worth noting that the contrast obtained by SEM is higher than the OM one. Image processing Gwyddion software facilitated estimating the covered area in that region, revealing a coverage C_{OM} = (60 ± 5) % by OM and C_{SEM} = (70 ± 5)% by SEM (see Fig. S3†). The higher contrast provided by SEM enables a more accurate and precise estimation of the

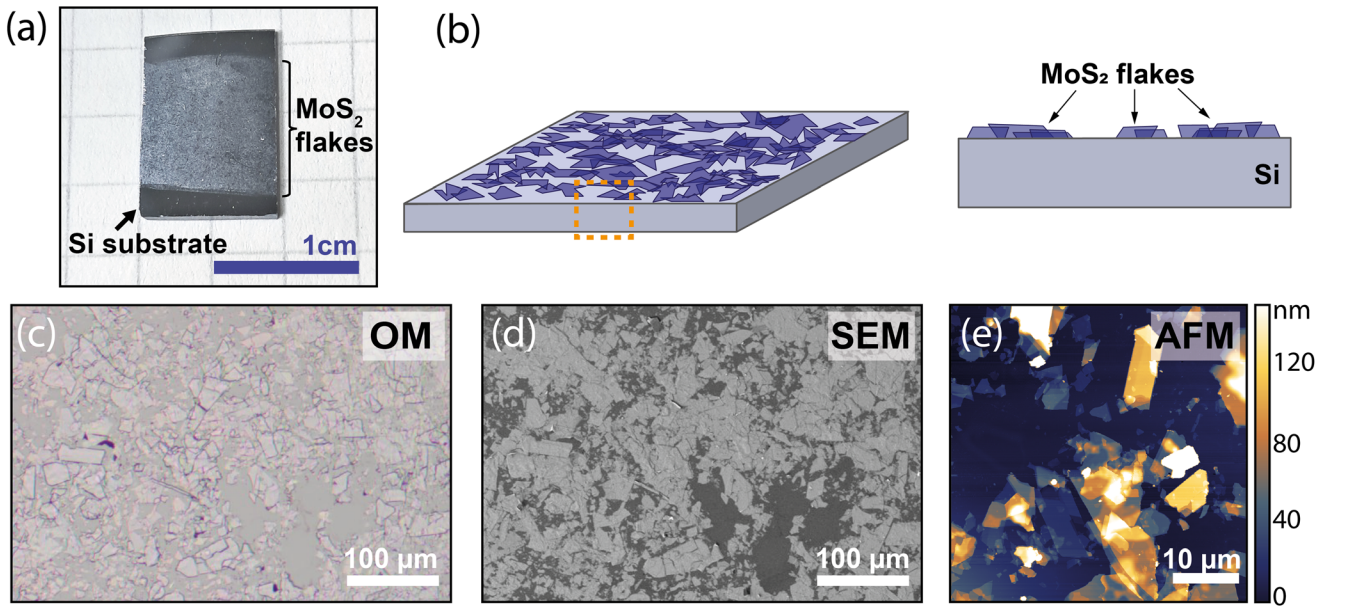

Fig. 1 (a) Photograph of the MoS_2 flakes transferred onto a Si substrate of approximately 1 cm^2. (b) Schematic representation of the deposited MoS_2 flakes. The right panel shows a lateral section. Optical (c) and scanning electron (d) microscopies in the same region of the sample. (e) AFM image of 45 × 45 μm^2.

covered area, as compared to OM, which depends on the refractive indexes of the vdW material and the substrate and on the thickness of the flakes. These findings were also obtained for Gr flakes noticing that, in that case, the SEM image provided an inverted contrast with respect to MoS_2 due to the higher conductivity of graphite compared to the Si substrate (see Fig. S4†).

We noted that the area covered along the sample can vary among regions (see Fig. S2c†). Thus, to get a more precise estimation of the area covered, several optical images were acquired in different sample regions and analysed, yielding an average value of C_{OM} = (55 ± 5)% for the MoS_2 sample. Even though this value provides a lower limit for the coverage, as discussed before, it offers insights into the fraction of area covered by the MoS_2 flakes.

Finally, AFM imaging (Fig. 1e) shows that the height of the transferred flakes, with an average value of approximately 90 nm (see Fig. S5†), is in good agreement with the reported value by Y. Sozen *et al.*[15] We noticed that this thickness is larger than the typical probing depth of XPS for the photon energies used in the research, which is in the order of 1–3 nm.[21–23]

After the morphological characterisation, we proceed to analyse the MoS_2 transferred sample using XPS. Fig. 2a displays the survey spectrum of the sample after 12 hours of annealing in UHV at 150 °C, revealing distinct peaks ascribed to MoS_2 and Si/SiO_2, as labelled in Fig. 2a. Eventually, peaks ascribed to Ta are also observed, coming from the Ta strips that hold the sample in place.

By the analysis of the areas of the core levels, normalised to their cross sections, coming from the substrate (Si and O) and of the ones coming from the material under investigation (Mo, S) we were able to estimate a coverage of C_{XPS} = (70 ± 5)%. This result is in good agreement with the results obtained by SEM and OM. It can be then concluded that the analysis of the coverage by morphological techniques, such as SEM or OM, or compositional techniques, such as XPS, point out to a similar coverage of the MoS_2 flakes on the Si substrate. Considering the various error sources for the different techniques, the coverages estimated in the three cases are well in agreement with each other (C_{OM} = (55 ± 5)%, C_{SEM} = (70 ± 5)%, C_{XPS} = (70 ± 5)%).

A second MoS_2 sample obtained with a single transfer (C_{OM} = (17 ± 5)%) was also subjected to XPS analysis. Despite the low coverage, well-defined signals were recorded for the survey and single spectra (see Fig. S6 and S7†). In addition, the coverage by XPS was also obtained by comparing the areas of the Mo and S peaks with the ones of Si and O finding a coverage of C_{XPS} = (25 ± 5)%. The good agreement between the OM and XPS estimated coverage is consistent with the previously discussed MoS_2 sample showing a higher coverage. A further discussion about this aspect and about the inelastic peak shape analysis[24–26] can be found in the ESI (Fig. S8 and S9†).

A detailed examination of the Mo 3d, S 2p, and Si 2p core levels peaks is provided in Fig. 2b, c and d, respectively and in Table S1.† It is noticed the presence of the Mo^{4+} 3d spin–orbit split doublet (at 229.8 eV and 233.0 eV for the $3d_{5/2}$ and $3d_{3/2}$) and the presence of S 2s (227.1 eV) core levels,[27–31] with no Mo^{6+} components indicative of molybdenum oxide,[27] confirming material purity. The S 2p region displays its corresponding spin–orbit ($2p_{3/2}$ at 162.6 eV and $2p_{1/2}$ at 163.8 eV),[27,30] while the Si 2p region exhibits the two Si $2p_{3/2}$ (99.7 eV) and Si $2p_{1/2}$

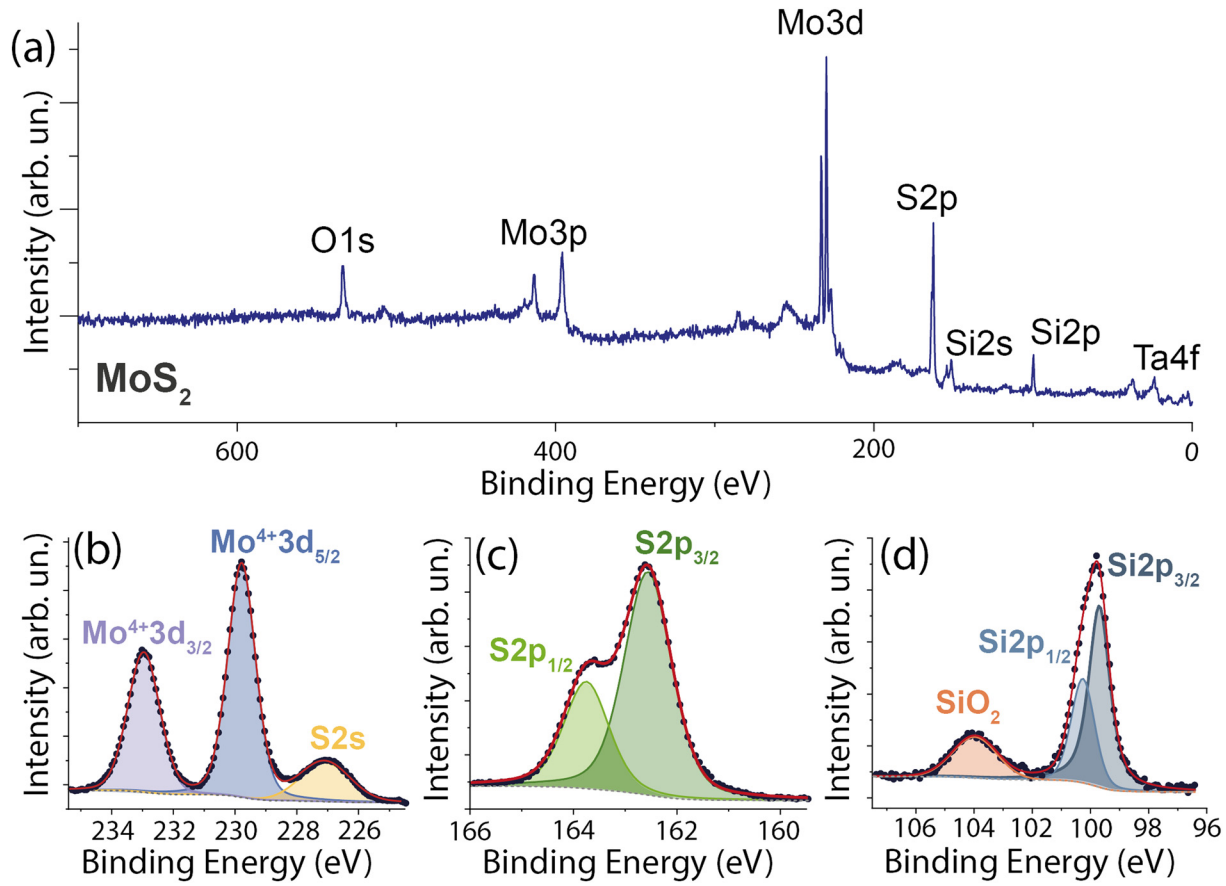

Fig. 2 XPS results for the MoS_2 sample transferred onto a Si substrate. (a) Survey spectrum indicating the corresponding peaks with tags. Mo 3d and S 2s (b), S 2p (c) and Si 2p (d) core levels. Experimental data indicated with dots, total fit in red, and Shirley background with a dashed dotted line. The individual peaks are coloured and their corresponding core-levels are indicated in the figure. Fitting parameters can be found in Table S1.† Spectra were recorded with a photon energy $h\nu$ = 1253.6 eV and a PE of 50 eV.

(100.3 eV) spin–orbit split doublet[32,33] along with a peak centred at 104.0 eV attributed to the SiO_2 component,[32,33] indicating the presence of surface oxide on Si.

Finally, it is noteworthy the presence of a tiny C 1s peak at around 285.5 eV in the survey spectrum (see Fig. 2a) in comparison with the core levels of the MoS_2 flakes. The energy of this peak points to some hydroxide and oxide carbon species[34,35] that could indicate the presence of residues from the Nitto tape on top of the transferred flakes or on the substrate. However, this small carbon/molybdenum ratio highlights the cleanliness of the technique employed, despite using a polymeric glue tape and high temperatures, suggesting that the presence of residue and contaminants is minimal.

To demonstrate the general nature and applicability of this technique to various vdW materials, graphite flakes and WSe_2 flakes were also deposited onto Si wafers. The morphological characterisation can be found in the ESI (Fig. S4 and S10†). Fig. 3 displays the survey spectra and the main core levels of these two compounds.

In the case of the graphite sample (Fig. 3a and b), a distinct and well-defined peak centred at 284.8 eV is observed,[34] along with a shoulder at 285.9 eV corresponding to the oxidised states of carbon and other functionalization groups.[34,35] The contribution of this oxide component is 18.5%. Nevertheless, the intensity of this C 1s core level is significantly higher than in the other vdW materials under investigation (as evidenced in Fig. 3a), and the main peak at 284.8 eV indicates a clear presence of sp^2 carbon, as expected for Gr flakes.[36] The coverage of this sample is C_{OM} = (45 ± 5)%, C_{SEM} = (34 ± 5)%, and C_{XPS} = (36 ± 5)% consistent with the previous results of coverage obtained for MoS_2.

Additionally, these results were compared with those of highly oriented pyrolytic graphite (HOPG) measured in the same XPS apparatus. HOPG is the most similar bulk system to the Gr-flakes under investigation in this research, as it is composed of layers of graphite crystallites highly oriented along the *c* axis. In Fig. S11a,† it can be observed that the line shapes of these two graphitic materials closely match. The analysis of the residual difference signal (Fig. S11b†) between these two fits highlights differences at BE above 285.5 eV which is compatible with the presence of functionalized groups, such as hydrocarbons, carbon hydroxides and oxides at higher binding energy,[34–36] in the case of Gr-flakes. This is presumably due to a higher density of edges caused by the finite size of the

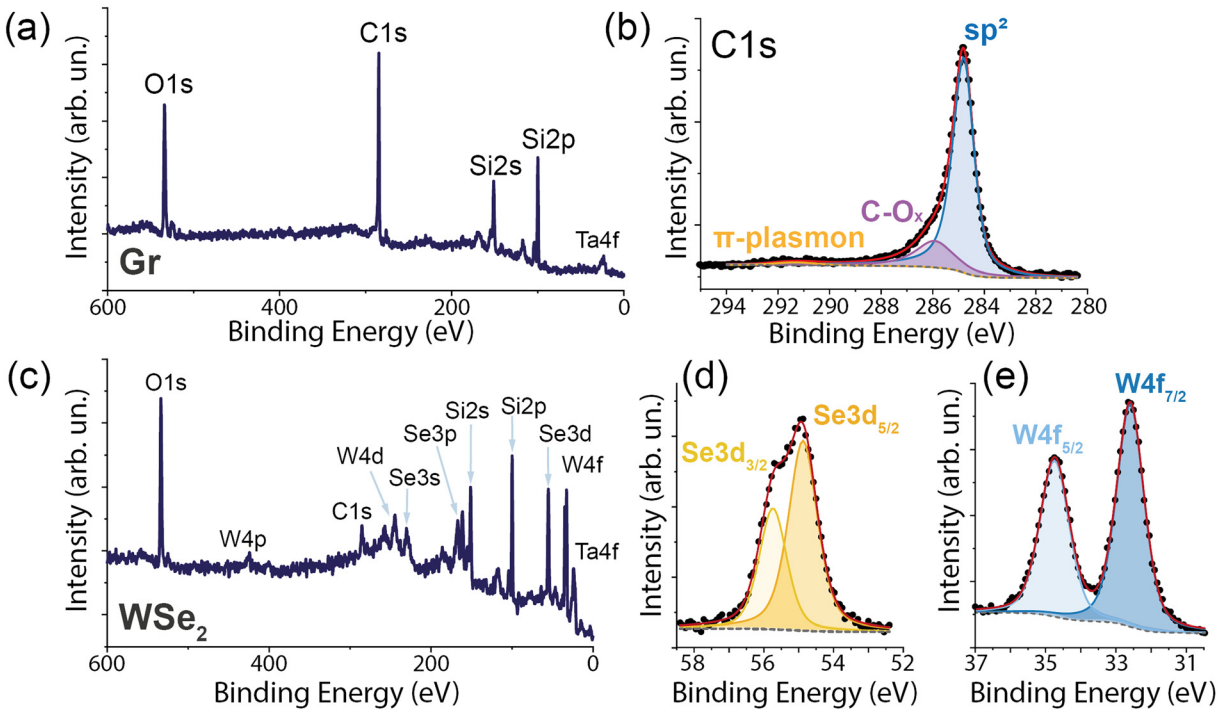

Fig. 3 (a) Survey spectrum for Gr sample and (b) C 1s core level. (c) Survey spectrum for WSe_2 sample and (d) Se 3d and (e) W 4f core levels. Experimental data indicated with dots, total fit in red, and Shirley background with a dashed dotted line. The individual peaks are coloured and their corresponding core level is indicated in the figure. Fitting parameters can be found in Tables S2 and S3.† Spectra were recorded with a photon energy $h\nu$ = 1253.6 eV and a PE of 50 eV.

flakes, with respect to the large terraces present in HOPG. Overall, these results are a good validation of this high-throughput massive exfoliation of vdW materials to measure the XPS spectra.

Tungsten diselenide (WSe_2) was also analysed by XPS (see Fig. 3c–e). A significant number of core levels ascribed to this compound were recorded in the survey spectrum (Fig. 3c). We focused on measuring the two most intense peaks of each element with high-resolution, which are the Se 3d (Fig. 3d) and the W 4f[37–39] (Fig. 3e). Both core-levels show their characteristic spin orbit doublets Se $3d_{5/2}$ (54.8 eV), Se $3d_{3/2}$ (55.7 eV) and W $4f_{7/2}$ (32.6 eV), W $4f_{5/2}$ (34.7 eV),[37–40] with the absence of oxide components.[40]

Lastly, $FePS_3$, a magnetic vdW material, was investigated. The peculiarity of this compound is that, unlike the others explored in this work, it was synthesised by some of the authors of the present manuscript. This made this sample of particular interest for elemental investigation and to check the presence of eventual contaminants. Moreover, $FePS_3$ is known in literature for its sensitivity to oxygen species and its tendency to degrade in air,[41,42] prompting us to investigate its degradation using XPS.

$FePS_3$ was first transferred onto a Si wafer using the technique reported in the experimental section, conducted in ambient atmosphere. After analysing the composition of the compound by XPS, we observed the signal from some oxide peaks (see ESI, Fig. S12†). However, whether the oxidation occurred during the transfer method or during the synthesis remained uncertain. To address this uncertainty, we fabricated a second sample performing the exfoliation and transfer of $FePS_3$ inside a gloveless anaerobic chamber[43] filled with an inert N_2 atmosphere. The results obtained for this last sample are reported in Fig. 4.

Fig. 4a presents the survey spectrum for the as-prepared $FePS_3$ sample. Peaks ascribed to this compound are labelled in the figure, evidencing the lack of contamination from unexpected elements and the lack of oxides observed in the sample prepared in air, evidencing the necessity to use inert atmospheres when transferring air-sensitive compounds.

The deconvoluted high-resolution XPS spectrum of $FePS_3$ shows the typical Fe 2p line shape.[44–49] Peaks at 709.2 eV and 722.7 eV correspond to the $2p_{3/2}$ and $2p_{1/2}$ core levels of Fe^{2+},[44,46,48–50] respectively, and peaks at 710.9 eV and 723.7 eV correspond to the Fe^{3+} $2p_{3/2}$ and $2p_{1/2}$,[46,47,50] respectively. In addition, two satellite peaks are present in the recorded spectrum, already observed and reported for this compound.[45,46] The S 2p core level shows the S 2p spin–orbit split doublet at 162.4 eV and 163.5 eV,[48,50] which is slightly shifted towards higher binding energies compared to other works in literature[44,46,51] but agrees well with the results reported for electrochemically-exfoliated $FePS_3$[49] and mechanically exfoliated $FePS_3$ by mortar grinding.[50] A broad peak was also observed at around 168.5 eV due to the presence of oxides and sulfates.[44,49,52] The P 2p core level evidences the spin–orbit doublet at 131.8 eV and 132.7 eV.[44,46–49,51]

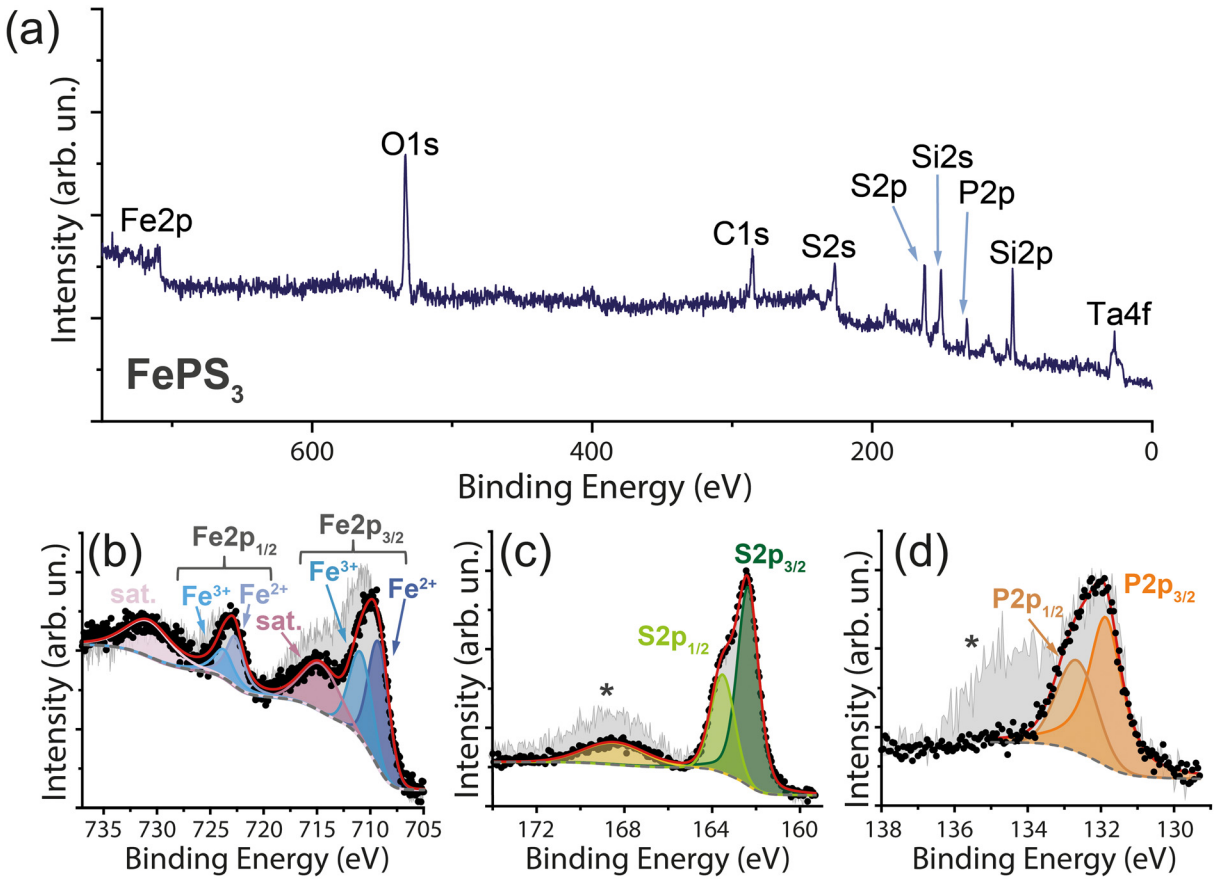

Fig. 4 XPS results for the $FePS_3$ sample transferred onto a Si substrate. (a) Survey spectrum indicating the corresponding peaks with tags. Fe 2p (b), S 2p (c) and P 2p (d) core levels. Experimental data indicated with dots, total fit in red, and Shirley background with a dashed dotted line. The individual peaks are coloured and their corresponding core-level is indicated in the figure. The grey shadowed line-shape present in the panels (b), (c), and (d) corresponds to the data recorded for the same sample after storing it in air for 20 days. * peaks ascribed to oxygen bonds as discussed in the text. Fitting parameters can be found in Table S4.† Spectra were recorded with a photon energy $h\nu$ = 1468.7 eV and a PE of 50 eV.

The stability of the compound was further investigated after storing it in air at room temperature for 7 and 20 days. After 7 days, the XPS spectra remained consistent with the as-prepared samples (see Fig. S12†), therefore showing no sign of degradation in this time scale. This result is consistent with previous reports on mechanically exfoliated $FePS_3$ flakes that demonstrated stability for 6 days by Raman spectroscopy.[41] However, degradation was observed after 20 days, with noticeable changes in the Fe 2p, S 2p and P 2p core levels (see Fig. 4b–d), also consistent with the degradation of the optoelectronic properties of devices based on $FePS_3$ flakes after some weeks in ambient conditions.[42] An increase in the 168.5 eV peak in the S 2p suggests the appearance of sulfates and oxides. Furthermore, we observe a strong change in the P 2p core level with the emergence of an intense peak around 134 eV, also observed on the sample prepared in air (see Fig. S12†), which is ascribed to phosphorous oxide.[46,47,53] Finally, the Fe 2p peak increases in intensity and slightly shifts to higher binding energies, probably also due to the presence of oxygen bonds.[54,55]

Overall, characterising air-sensitive $FePS_3$ by XPS highlights the necessity of employing inert atmospheres when transferring this type of materials through massive parallel heat-assisted exfoliation. Additionally, this work underscores the utility of evaluating the quality of exfoliated vdW materials, as their chemical composition can be modified drastically in short periods of time, thereby impacting the research results.

Conclusions

In this research, we have successfully demonstrated the use of X-ray photoelectron spectroscopy to investigate the chemical composition of van der Waals materials. VdW flakes have been deposited over Si wafers in areas of about 1 cm^2 using little quantities of material (around 10 μg). Our findings evidence that even with minimal coverage, XPS provides excellent resolution. The survey spectra and highly resolved core levels have been recorded to determine the chemical composition of MoS_2, graphite, WSe_2 and $FePS_3$, which agrees with the literature published until now. In addition, we have shown that when working with air-sensitive materials, such as $FePS_3$, the

transfer method needs to be conducted in an inert atmosphere to prevent sample oxidation.

This work opens up the possibility of controlling the purity of commercial materials and assessing the damage caused by air exposure or other induced modifications. At the same time, it is an easy and straightforward technique for facilitating comparisons of the same 2D materials across different research groups.

Data availability

The data that support the findings of this research are available from the authors upon reasonable request.

Conflicts of interest

There are no conflicts to declare.

Acknowledgements

This research was partially funded by the European Union-Next Generation EU under the PRIN Grants 2D-FRONTIERS (20228879FT), 2D-PentaSensing (P2022HT3FF) and ANDROMeDA (PRIN_2020Y2JMP5) of MUR, by the INFN Ptolemy project, EC project ATTRACT (Grant Agreement 777222), PID2021-126098OB-I00/AEI/FEDER10.13039/501100011033 grant of Spanish MICINN, and by Sapienza University Ateneo and “Avvio alla Ricerca” and "Ateneo" funds.

References

1 Z. Cui, *et al.*, Electronic and optical properties of van der Waals heterostructures of g-GaN and transition metal dichalcogenides, *Appl. Surf. Sci.*, 2019, **492**, 513–519.
2 W. Zhang, *et al.*, Integrating van der Waals materials on paper substrates for electrical and optical applications, *Appl. Mater. Today*, 2021, **23**, 101012.
3 J. Shang, *et al.*, Tunable electronic and optical properties of InSe/InTe van der Waals heterostructures toward optoelectronic applications, *J. Mater. Chem. C*, 2018, **6**, 7201–7206.
4 J. He, *et al.*, 2D van der Waals heterostructures: processing, optical properties and applications in ultrafast photonics, *Mater. Horiz.*, 2020, **7**, 2903–2921.
5 Y. Qi, *et al.*, Recent Progress in Strain Engineering on van der Waals 2D Materials: Tunable Electrical, Electrochemical, Magnetic, and Optical Properties, *Adv. Mater.*, 2023, **35**, 2205714.
6 G. Wang, *et al.*, Bending of Multilayer van der Waals Materials, *Phys. Rev. Lett.*, 2019, **123**, 116101.
7 R. Frisenda, Y. Niu, P. Gant, M. Muñoz and A. Castellanos-Gomez, Naturally occurring van der Waals materials, *npj 2D Mater. Appl.*, 2020, **4**, 38.
8 F. Miao, S.-J. Liang and B. Cheng, Straintronics with van der Waals materials, *npj Quantum Mater.*, 2021, **6**, 59.
9 E. Gao, *et al.*, Mechanical exfoliation of two-dimensional materials, *J. Mech. Phys. Solids*, 2018, **115**, 248–262.
10 M. Onodera, S. Masubuchi, R. Moriya and T. Machida, Assembly of van der Waals heterostructures: exfoliation, searching, and stacking of 2D materials, *Jpn. J. Appl. Phys.*, 2020, **59**, 010101.
11 F. Liu, Mechanical exfoliation of large area 2D materials from vdW crystals, *Prog. Surf. Sci.*, 2021, **96**, 100626.
12 F. Bonaccorso, *et al.*, Production and processing of graphene and 2d crystals, *Mater. Today*, 2012, **15**, 564–589.
13 K. DiCamillo, S. Krylyuk, W. Shi, A. Davydov and M. Paranjape, Automated Mechanical Exfoliation of MoS2 and MoTe2 Layers for Two-Dimensional Materials Applications, *IEEE Trans. Nanotechnol.*, 2019, **18**, 144–148.
14 J. Chen, M. Duan and G. Chen, Continuous mechanical exfoliation of graphene sheets via three-roll mill, *J. Mater. Chem.*, 2012, **22**, 19625.
15 Y. Sozen, J. J. Riquelme, Y. Xie, C. Munuera and A. Castellanos-Gomez, High–Throughput Mechanical Exfoliation for Low–Cost Production of van der Waals Nanosheets, *Small Methods*, 2023, **7**, 2300326.
16 M. Chen, *et al.*, Nanoimprint-Assisted Shear Exfoliation (NASE) for Producing Multilayer MoS2 Structures as Field-Effect Transistor Channel Arrays, *ACS Nano*, 2015, **9**, 8773–8785.
17 F. A. Stevie and C. L. Donley, Introduction to X-ray photoelectron spectroscopy, *J. Vac. Sci. Technol., A*, 2020, **38**, 063204.
18 G. H. Major, *et al.*, Practical guide for curve fitting in X-ray photoelectron spectroscopy, *J. Vac. Sci. Technol., A*, 2020, **38**, 061203.
19 D. R. Baer, *et al.*, Practical guides for X-ray photoelectron spectroscopy: First steps in planning, conducting, and reporting XPS measurements, *J. Vac. Sci. Technol., A*, 2019, **37**, 031401.
20 C. Ernandes, *et al.*, Indirect to direct band gap crossover in two-dimensional WS2(1−x)Se2x alloys, *npj 2D Mater. Appl.*, 2021, **5**, 7.
21 M. P. Seah and W. A. Dench, Quantitative electron spectroscopy of surfaces: A standard data base for electron inelastic mean free paths in solids, *Surf. Interface Anal.*, 1979, **1**, 2–11.
22 C. J. Powell, Practical guide for inelastic mean free paths, effective attenuation lengths, mean escape depths, and information depths in X-ray photoelectron spectroscopy, *J. Vac. Sci. Technol., A*, 2020, **38**, 023209.
23 H. Shinotsuka, S. Tanuma, C. J. Powell and D. R. Penn, Calculations of electron inelastic mean free paths. XII. Data for 42 inorganic compounds over the 50 eV to 200 keV range with the full Penn algorithm, *Surf. Interface Anal.*, 2019, **51**, 427–457.
24 S. Tougaard, Improved XPS analysis by visual inspection of the survey spectrum, *Surf. Interface Anal.*, 2018, **50**, 657–666.

25 S. Tougaard, Practical guide to the use of backgrounds in quantitative XPS, *J. Vac. Sci. Technol., A*, 2021, **39**, 011201.
26 A. Herrera-Gomez, M. Bravo-Sanchez, F. S. Aguirre-Tostado and M. O. Vazquez-Lepe, The slope-background for the near-peak regimen of photoemission spectra, *J. Electron Spectrosc. Relat. Phenom.*, 2013, **189**, 76–80.
27 N. Jiménez-Arévalo, *et al.*, MoS2 Photoelectrodes for Hydrogen Production: Tuning the S-Vacancy Content in Highly Homogeneous Ultrathin Nanocrystals, *ACS Appl. Mater. Interfaces*, 2023, **15**, 33514–33524.
28 N. H. Turner and A. M. Singlet, Determination of Peak Positions and Areas from Wide-scan XPS Spectra", *Surf. Interface Anal.*, 1990, **15**, 215–222.
29 D. Ganta, S. Sinha and R. T. Haasch, 2-D Material Molybdenum Disulfide Analyzed by XPS, *Surf. Sci. Spectra*, 2014, **21**, 19–27.
30 D. Qiu, D. U. Lee, S. W. Pak and E. K. Kim, Structural and optical properties of MoS2 layers grown by successive two-step chemical vapor deposition method, *Thin Solid Films*, 2015, **587**, 47–51.
31 S. Hussain, *et al.*, Large-area, continuous and high electrical performances of bilayer to few layers MoS2 fabricated by RF sputtering via post-deposition annealing method, *Sci. Rep.*, 2016, **6**, 30791.
32 M. Czernohorsky, *et al.*, High-K metal gate stacks with ultra-thin interfacial layers formed by low temperature microwave-based plasma oxidation, *Microelectron. Eng.*, 2017, **178**, 262–265.
33 L. Zhang, N. Kuramoto, Y. Azuma, A. Kurokawa and K. Fujii, Thickness Measurement of Oxide and Carbonaceous Layers on a 28Si Sphere by XPS, *IEEE Trans. Instrum. Meas.*, 2017, **66**, 1297–1303.
34 X. Chen, X. Wang and D. Fang, A review on C1s XPS-spectra for some kinds of carbon materials, *Fullerenes, Nanotubes Carbon Nanostruct.*, 2020, **28**, 1048–1058.
35 I.-Y. Jeon, *et al.*, Edge-carboxylated graphene nanosheets via ball milling, *Proc. Natl. Acad. Sci. U. S. A.*, 2012, **109**, 5588–5593.
36 L. Wei, *et al.*, Spontaneous intercalation of long-chain alkyl ammonium into edge-selectively oxidized graphite to efficiently produce high-quality graphene, *Sci. Rep.*, 2013, **3**, 2636.
37 G. Salitra, G. Hodes, E. Klein and R. Tenne, Highly oriented WSe2 thin films prepared by selenization of evaporated WO3, *Thin Solid Films*, 1994, **245**, 180–185.
38 J.-K. Huang, *et al.*, Large-Area Synthesis of Highly Crystalline WSe2 Monolayers and Device Applications, *ACS Nano*, 2014, **8**, 923–930.
39 Y. Duan, S. Feng, K. Zhang, J. Qiu and S. Zhang, Vertical Few-Layer WSe2 Nanosheets for NO2 Sensing, *ACS Appl. Nano Mater.*, 2021, **4**, 12043–12050.
40 M. Yamamoto, *et al.*, Self-Limiting Layer-by-Layer Oxidation of Atomically Thin WSe2, *Nano Lett.*, 2015, **15**, 2067–2073.
41 J. U. Lee, *et al.*, Ising-Type Magnetic Ordering in Atomically Thin FePS3, *Nano Lett.*, 2016, **16**, 7433–7438.
42 M. Ramos, *et al.*, Ultra-broad spectral photo-response in FePS3 air-stable devices, *npj 2D Mater. Appl.*, 2021, **5**, 19.
43 P. Gant, *et al.*, A system for the deterministic transfer of 2D materials under inert environmental conditions, *2D Mater.*, 2020, **7**, 025034.
44 Y. Ding, *et al.*, Facile Synthesis of FePS3 Nanosheets@MXene Composite as a High-Performance Anode Material for Sodium Storage, *Nano-Micro Lett.*, 2020, **12**, 54.
45 H. Huang, *et al.*, Few-layer FePS3 decorated with thin MoS2 nanosheets for efficient hydrogen evolution reaction in alkaline and acidic media, *Appl. Surf. Sci.*, 2020, **525**, 146623.
46 D. Mukherjee, P. M. Austeria and S. Sampath, Two-Dimensional, Few-Layer Phosphochalcogenide, FePS3 : A New Catalyst for Electrochemical Hydrogen Evolution over Wide pH Range, *ACS Energy Lett.*, 2016, **1**, 367–372.
47 Q. Qin, *et al.*, A Tannic Acid–Derived N–, P–Codoped Carbon–Supported Iron–Based Nanocomposite as an Advanced Trifunctional Electrocatalyst for the Overall Water Splitting Cells and Zinc–Air Batteries, *Adv. Energy Mater.*, 2019, **9**, 1803312.
48 K. Ichimura and M. Sano, Electrical conductivity of layered transition-metal phosphorus trisulfide crystals, *Synth. Met.*, 1991, **45**, 203–211.
49 H. Wang, *et al.*, An exfoliated iron phosphorus trisulfide nanosheet with rich sulfur vacancy for efficient dinitrogen fixation and Zn-N2 battery, *Nano Energy*, 2021, **81**, 105613.
50 Y. Zhang, *et al.*, Exfoliated FePS3 nanosheets for T1-weighted magnetic resonance imaging-guided near-infrared photothermal therapy in vivo, *Sci. China Mater.*, 2021, **64**, 2613–2623.
51 Y. Jin, *et al.*, To the Stability of Janus Phases in Layered Trichalcogenide MPX3 Crystals: Insights from Experiments and Theory, *J. Phys. Chem. C*, 2022, **126**, 16061–16068.
52 Y. Ma, *et al.*, Rational design of few-layer FePS3 nanosheets@N-doped carbon composites as anodes for sodium-ion batteries, *Chem. Eng. J.*, 2022, **427**, 130882.
53 G. Chen, *et al.*, Efficient and Stable Bifunctional Electrocatalysts Ni/NixMy (M = P, S) for Overall Water Splitting, *Adv. Funct. Mater.*, 2016, **26**, 3314–3323.
54 Y. He, *et al.*, Iron-Based Oxygen Scavengers on Mesoporous Silica Nanospheres, *ACS Omega*, 2023, **8**, 21689–21695.
55 Z. Swiatkowska-Warkocka, K. Kawaguchi, H. Wang, Y. Katou and N. Koshizaki, Controlling exchange bias in Fe3O4/FeO composite particles prepared by pulsed laser irradiation, *Nanoscale Res. Lett.*, 2011, **6**, 226.